Force model in the penetration by impact into confined granular media

Antoine Seguin

Force model in the penetration by impact into confined granular media

A. Seguin[1]

[1] *Université Paris-Saclay, CNRS, FAST, 91405 Orsay, France*

Abstract –We study analytically the influence of lateral confinement on the penetration depth of a sphere into a granular medium by impact. The granular medium is contained in a cylindrical tank of diameter D and a sphere of diameter d plunges along its axis. The presence of side walls, parametrized by the distance $D-d$ between the walls and the sphere, influences the penetration depth. Here, we deploy a continuous analytical model to account for the presence of side walls. After solving and calibrating this model for an infinite medium ($D/d \to \infty$), we show that it is possible to extend this model without any additional parameters to account for lateral confinement. The influence of side walls is modelled by an exponential effect, which modifies the sphere's penetration dynamics. The solution of the model is shown to be in agreement with experimental results.

Introduction. – The impact pattern of objects on materials is a recurring problem to measure the energy that the materials are capable of absorbing during an impact. Beyond mechanical testing, soil mechanics and geotechnics, this generic configuration has industrial applications [1, 2] and geological applications in the formation of impact craters [3, 4, 5]. To study these configurations, divided media such as granular materials are often used at laboratory scale [6, 7, 8, 9, 10, 11, 12, 13, 14]. When a sphere of diameter d and density ρ impacts a granular material of density ρ_g, the sphere ejects grains from the medium on impact, penetrates the medium and comes to rest at a depth defined by the geometric and kinetic parameters of both the sphere and the granular medium. The penetration depth δ has been extensively studied in previous studies. To characterize δ as a function of the kinetic energy imparted to the sphere, most of the usual scaling laws use the total height of fall h [7, 8, 15, 16, 17]. This total height of fall h is the sum of the height during free fall and the penetration depth δ. The decision to use the height h is motivated by energy considerations. During penetration, the projectile still possesses non-zero kinetic energy, and often travels a distance greater than its diameter. In this case δ is not negligible compared with the free fall height. Therefore the kinetic energy of the projectile dissipated along δ is taken into account in an effective total height of fall h. A commonly used scaling law has the following expression:

$$\frac{\delta}{d} = A \left(\frac{\rho}{\rho_g}\right)^{\beta} \left(\frac{h}{d}\right)^{\alpha} \tag{1}$$

where α and β are exponents determined experimentally [7, 8]. It is also possible to choose the impact velocity v_i as parameter in order to develop an other scaling law [15]. This approximate scaling law is a practical formulation whereas others models for infinite media typically gives an implicit formulation through the equation of the object's penetration dynamics [18, 19, 20, 21]. The final impact depth δ is linked to the dynamics of the sphere during it penetration over time. Thus, during its path, the granular medium exerts a global drag force on the object, leading to its stop. The drag force of an object in a granular medium is often modelled by the sum of two terms [18, 19]: a frictional drag term and a collisional drag term. The frictional drag term is modelled by a force proportional to the pressure prevailing in the granular medium [22, 23] whereas the collisional drag term is characterized by the resistance to advancement produced by the dissipation of kinetic energy when grains collide with the object [18, 19, 24, 25].

Most real-life geotechnical or industrial situations involve walls that can alter the penetration of objects. It is thus important to understand and anticipate how the wall will affect the object's penetration. Most of the time, the granular medium is considered as infinite medium.

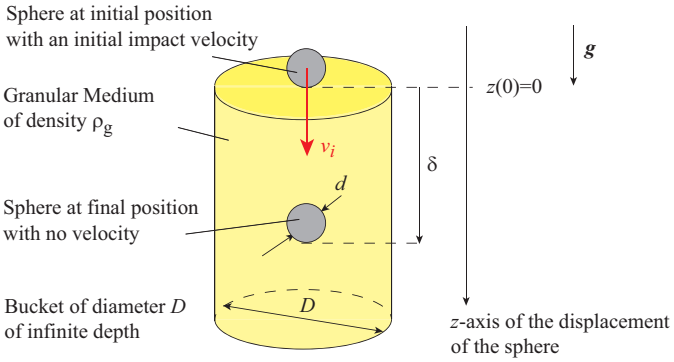

Fig. 1: Sketch of the studied configuration defining the main parameters of the model.

A first study has defined the geometric conditions to be met by experiments in granular materials in order to determine whether wall effects can be neglected. [8]. The influence of walls has the effect of decreasing the depth of penetration as confinement becomes more and more significant. This lateral confinement effect is reflected in the values of the exponent α and the prefactor A of equation 1, which are functions of the size of the container of the granular medium. As confinement increases, the values of α and A decrease. However these evolutions remain descriptive and there is no analytical model to take this effect into account.

In this paper, we develop and propose a model of the influence of lateral confinement during impact penetration in a granular material. After the presentation of the model configuration, we establish the general equation for the penetration dynamics of a sphere in a laterally confined granular material. We first describe the different models of drag terms already observed in various configurations. Then we combine all these terms to define a general equation for penetration dynamics. This equation includes a new term accounting for the lateral confinement. After fitting the model on experimental results obtained in infinite granular media, we show that this model provides valid results for laterally confined granular media.

Configuration. – The configuration is shown in figure 1. A sphere of diameter d, density ρ and mass $m = \pi\rho d^3/6$ impacts vertically with a granular medium at impact velocity v_i. Thus, this impact velocity v_i comes from a free fall drop at a height ${v_i}^2/(2g)$ where g is the gravity field. After this impact (corresponding to the surface of the granular material and the origin of the displacement), the sphere moves through the granular medium at a depth $z(t)$ which increases as a function of time until it stops at a depth δ. The granular medium is considered to be a model continuous medium whose constituent grains have a density ρ_g, so the diameter of the grains are not taken into account. The packing fraction is assumed to be constant and homogeneous throughout the object's penetration. The granular medium is contained in a cylindrical container of diameter D and infinite height. It has been shown experimentally that the bottom of the tank has no influence on penetration depth [8]. The goal is to determine the final penetration depth δ as a function of all geometric parameters, material parameters and impact velocity. We thus define the total height of fall $h = \delta + {v_i}^2/(2g)$.

The penetration dynamics $z(t)$ is based on two sources of drag forces. The first term comes from a frictional drag force resulting from a local shear stress proportional to pressure [22, 23]. As the pressure in the granular material is hydrostatic, this pressure is modeled by a term $\sim \rho_g g z$, where z is the instantaneous depth. The second term comes from an inertial drag force resulting from collisions. The stress generated by these collisions is modelled by a term $\sim \rho_g (dz/dt)^2$ where dz/dt represents the vertical velocity of the object.

Confined granular media have also been the subject of numerous studies [8, 26, 27, 28, 29, 30]. More generally, the effect of confinement of granular media was highlighted by Janssen's pioneering work [31]. When a granular medium is used to fill a tank, the pressure at the bottom of the tank does not evolve linearly with the weight of the grain column, but saturates at a constant value. This saturation is generated by the fact that the grains exhibits a non-zero friction coefficient and cling to the walls of the tank. The weight of the grains is then taken up by the side walls, and there is a skimming length characteristic of this saturation, linked to the characteristic dimension of the tank. This effect, known as the Janssen effect, also exists in a dynamic version when there is relative movement between the walls and the grains [27]. This saturation exists when the direction of relative motion is opposite to that of gravity. However, the direction has a strong influence on the modeling and on the intensity of this effect [26]. When relative motion is in the direction of gravity, there is no saturation, but rather an amplification of the resistance force due to the walls. The stress formulation of this effect is modelled by a term $\sim \rho_g g \lambda \exp[(z/\lambda) - 1]$ where λ is an effective screening length [26].

Experimental data have already been established in the configuration of figure 1 in [8]. We reuse this data set for the comparison with our model. The granular bed is composed of glass spheres ($\rho_g \simeq 2500$ kg.m$^-$3) of mean diameter of 350 μm. Several tank of diameter D =24, 35, 40, 50, 62, 80, 128 and 190 mm has been used. The impacting sphere is made of different material leading to ρ =1140, 2150, 2500, 7800 and 14970 kg.m$^-$3. The sphere diameter is d =5, 10, 19, 20 and 40 mm. The velocity of impact v_i ranges from 0 to 3 m.s^{-1}.

Model. – In this configuration, we seek to determine the equation for the dynamics of the sphere as it moves through the granular medium. The force balance is made up of a driving force and two drag force terms, which have

the effect of slowing down the sphere. The driving force corresponds to the sphere's weight mg. According to previous studies [18, 19, 20, 21], the collisional drag force term can be reasonably modelled by an expression of the form $K_v\rho_g d^2(dz/dt)^2$ where d^2 is proportionnal to the surface of the sphere and K_v is a coefficient. In our model, we modify here the frictionnal drag force which is usually a linear function of z [18, 20, 21].

Referring to the experimental study of [26], during penetration of the sphere, the frictional drag force felt by the sphere is caused by the quasi-horizontal redirection of stresses in the grains in the vicinity of the lower part of the sphere. These stresses will be dissipated by friction through chains of forces between the grains [32]. When the distance between the tank walls and the sphere is small, these chains of forces will cling to the walls also by friction. In a formalism similar to the Janssen effect, this wall friction exerts a pressure that varies exponentially with the depth z with a characteristic distance between the walls and the sphere. The effect is positive here, since the sphere's motion moves in the opposite direction to the frictional forces, amplifying these forces. The inclusion of the exponential effect in the frictional term enables this term to be rewritten more finely, since it must be compatible with all existing formulations. If we consider the sphere moving relatively to a fixed wall of the container, then a basic effective characteristic length λ can be written simply as $\lambda = D - d$. Rewriting the exponential formulation [26], the frictional drag term becomes $K_z\rho_g g(D-d)d^2\exp[(z/(D-d))-1]$ where d^2 is still proportionnal to the sphere surface and K_z is a coefficient.

The general equation for the object's dynamics can be formulated as follows:

$$\frac{1}{6}\pi\rho d^3\frac{d^2z}{dt^2} = \frac{1}{6}\pi\rho d^3 g - K_v\rho_g g d^2\left(\frac{dz}{dt}\right)^2 - K_z\rho_g g(D-d)d^2\left(\exp\left(\frac{z(t)}{D-d}\right)-1\right), \quad (2)$$

with the following initial conditions $z(0) = 0$ and $dz/dt(0) = v_i$ where v_i is the initial impact velocity of the sphere. Note that in the limit of laterally unconfined media ($D \to \infty$), we recover the usual results for the friction drag force term in $K_z\rho_g g z d^2$ by performing a first order Taylor expansion in $z/(D-d)$ of the exponential. Thus, this complete equation includes previous formulations established in earlier studies [18, 21]. In order to write a normalized equation, it is relevant to establish the normalized quantities of time T, depth Z, screening length Λ and impact velocity V_i:

$$Z = \frac{6\rho_g z}{\pi\rho d} \qquad T = \left(\frac{6\rho_g g}{\pi\rho d}\right)^{1/2} t$$
$$\Lambda = \frac{6\rho_g(D-d)}{\pi\rho d} \qquad V_i = \left(\frac{6\rho_g}{\pi\rho g d}\right)^{1/2} v_i. \quad (3)$$

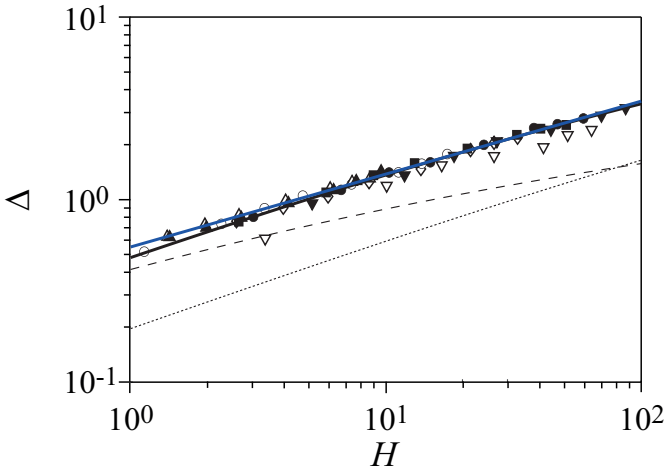

Fig. 2: Evolution of normalized penetration depth Δ as a function of normalized total height H. Experimental data for steel spheres $\rho = 7800$ kg.m^{-3} of different diameters: ($\triangledown$) $d = 5$ mm, $\diamond$ $d = 10$ mm, ($\circ$) $d = 20$ mm, and ($\triangle$) $d = 40$ mm. Experimental data for spheres of diameter $d = 20$ mm and of different materials corresponding to different density ratio ρ/ρ_g: ($\blacktriangledown$) $\rho = 1140$ kg.m^{-3}, ($\bullet$) $\rho = 2150$ kg.m^{-3}, ($\blacksquare$) $\rho = 2500$ kg.m^{-3} and ($\blacktriangle$) $\rho = 14970$ kg.m^{-3} [8]. The blue curve represents the fit of experimental data in infinite granular medium of the form $\Delta = BH^\alpha$ with $B = 0.55$ and $\alpha = 0.4$ [8]. The lines represents the solution of the equation 4 for $\Lambda \to \infty$ and for differents values of K_z and K_v: (plain line) $K_z = 8$ and $K_v = 0.15$, (dashed line) $K_z = 50$ and $K_v = 0.15$, (dotted line) $K_z = 8$ and $K_v = 1$.

By injecting these variables into equation 2, the normalized problem is then written:

$$\frac{d^2Z}{dT^2} = 1 - K_v\left(\frac{dZ}{dT}\right)^2 - K_z\Lambda\left(\exp\left(\frac{Z}{\Lambda}\right)-1\right), \quad (4)$$

with initial conditions $Z(0) = 0$ and $dZ/dT(0) = V_i$. Equation 4 can be solved numerically. The dimensionless distance Δ covered by the object from the granular surface ($Z(0) = 0$) until it stops can be evaluated when $dZ/dT = 0$.

Unbounded medium. – We first consider the case of an infinite tank corresponding to $D \to \infty$, thus $\Lambda \to \infty$ (Eq.3). The goal of this section is to determine the values of K_v and K_z that must be valid within this limit. It is important to note that the normalized variables provide the relationship $\delta/d = (\pi/6)(\rho/\rho_g)\Delta$ when the projectile stops (Eq. 3). Consequently, the total fall height is $h/d = (\pi/6)(\rho/\rho_g)(\Delta + V_i^2/2)$ allowing to define $H = \Delta + V_i^2/2$. In an infinite medium ($\Lambda \to \infty$), equation 4 reduces to the usual impact equation as $K_z\Lambda(\exp(Z/\Lambda) - 1) \sim K_z Z$ [18, 20, 21]. Thus, the penetration depth Δ is a function of the total height H such that $\Delta = f(H)$. As a result, the experimental scaling law 1 between δ and h can be improved. By injecting normalized quantities 3, the scaling

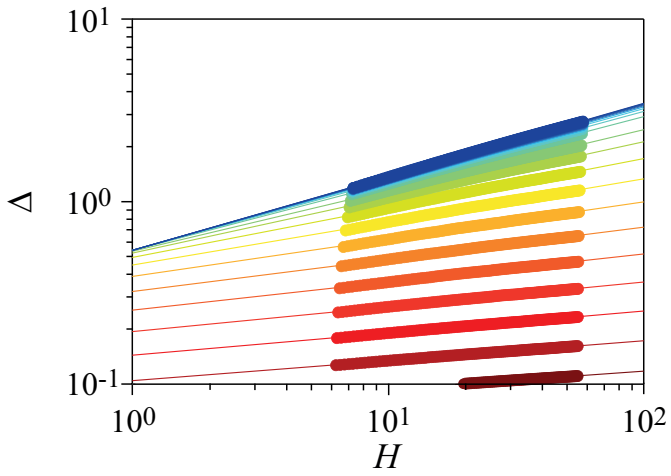

Fig. 3: Evolution of normalized penetration depth Δ as a function of normalized total head H. The large coloured curves represent the solution of the equation 4 for values $K_z = 8$ and $K_v = 0.15$ for different values of lateral confinement Λ. Color code spans from blue to red for $10^{-2} < \Lambda < 10$ respectively. The thin coloured curves represents a power law fit of the data using equation 6.

law 1 can be rewritten:

$$\Delta = A \left(\frac{6}{\pi}\right)^{1-\alpha} \left(\frac{\rho}{\rho_g}\right)^{\beta+\alpha-1} H^{\alpha} \qquad (5)$$

Since Δ depends only on H, this imposes the condition $\beta + \alpha = 1$. This result is exactly what was obtained experimentally [8, 15, 16]. Note that we can improve the relationship 1 by using the link between α and β. Therefore, equation 5 can be rewritten:

$$\Delta = BH^{\alpha} \qquad (6)$$

with $B = A\,(6/\pi)^{1-\alpha}$. Using the values obtained experimentally ($A = 0.37$ and $\alpha = 0.4$ [8]), this leads to $B \approx 0.55$. Note that B depends on α in this formulation. The coefficients K_z and K_v in equation 4 are coefficients characterizing energy dissipation in the medium. They include the various coefficients of friction and the collision dissipation coefficient. They are also a function of the packing fraction of the medium. The determination of these coefficients has been the subject of numerous studies [7, 19, 30, 33, 34, 35, 36].

We are working here on an experimental dataset obtained in an infinite granular medium corresponding to $D = 190$ mm [8]. The goal here is to make a comparison between the experimental measurements [8], the sclaing law given by the equation 6 and the solution of the equation 4 in the limit $\Lambda \to \infty$. Figure 2 shows those former experimental data by plotting Δ as a function of H. A power-law fit is applied on the experimental data (blue curve) according to equation 6 and this yields $\alpha = 0.4$ and $B = 0.55$. In parallel, we solve equation 4 for similar ranges of H (Fig. 2). The values $K_z = 8$ and $K_v = 0.15$ are used to draw the plain black curve in Fig. 2. We obtain excellent agreement with experimental measurements and recover the α and B values given by the fit of the experimental data. However relationship 6 is not the solution to the equation 4: we can only conclude that the difference between the two is small. Figure 2 shows the solution of equation 4 with $K_z = 8$ and $K_v = 1$ (dotted line) and with $K_z = 50$ and $K_v = 0.15$ (dashed line). The influence of K_z and K_v can be seen on the shape of the curves $\Delta = f(H)$. Note that B seems to be mainly a function of K_v (as the dotted line is almost parallel to the plain line) while α seems to be mainly a function of K_z (as the dashed line and the plain line are similar at low H values).

It is very likely that K_z and K_v depend on the packing fraction of the granular material. The evolution of the inertial drag force and the frictional drag force of a disk with an initial packing fraction ϕ_0 have been measured in a 2D packing [24, 25]. The two force terms vary as $(\phi_c - \phi_0)^{-1/2}$ where ϕ_c is the critical packing fraction. This formulation has geometrical origin, i.e. the disk needs extra space in order to move, so it creates a cluster in front of it. For an initial packing fraction close to the critical value ϕ_c, these forces diverge. In a 3D packing, we expect the two drag force terms to follow a similar dependency and therefore the coefficients K_z and K_v should vary such that $K_z \sim (\phi_c - \phi_0)^{-1/3}$ and $K_z \sim (\phi_c - \phi_0)^{-1/3}$. It is reasonable to assume that this formulation is only valid in the vicinity of the critical volume fraction $\phi_c \simeq 0.64$ (a reasonable value for 3D packing). Measurements of the figures 2 were carried out with an approximate value of $\phi_0 \simeq 0.60$. The experimental range of variation in ϕ_0 goes from loose to dense packing, i.e. $0.55 \leq \phi_0 \leq 0.63$. Thus, it is possible to give a range of coefficient varations with the packing fraction range ϕ_0 which is approximately $6.1 \leq K_z \leq 13.7$ and $0.11 \leq K_v \leq 0.26$. For the rest of our analytical study, $K_z = 8$ and $K_v = 0.15$ remain constant and there are no more adjustable parameters.

Lateral confinement of the medium. – We now investigate the influence of lateral confinement by evaluating the influence of the parameter Λ. To do this, we solve equation 4 for different values of Λ. The results are shown in figure 3 for intermediate H values with large plain line. The color scale ranges from red (low values of Λ) to blue ($\Lambda \to \infty$). We note that the lower the value of Λ, the lower the value of penetration Δ for a given value of H. This is in line with experimental observations [8].

In order to have a more explicit and synthetic comparison, we choose to model the analytical results provided by equation 6 in the partial range of H comparable to the experimental data. To do this, we fit the analytical data to equation 4. Thus, for each value of Λ, we determine the values of α and B. The fits are plotted on figure 3 with thin plain line on the all range of H.

Figure 4 shows the evolution of α and B as a function of Λ. It can be seen that α and B decrease as Λ decreases over the Λ range studied. Corresponding data points and fits from an earlier experimental study [8] have been added to figure 4: $\alpha = 0.4\,(1 - \exp(\Lambda/0.8))$ and $B = 0.37\ (\rho/\rho_g)^{0.61}\ ((\pi\rho)/(6\rho_g))^{1-\alpha}\ (1 - \exp(-(\Lambda(\pi\rho)/(6\rho_g) + 1)/0.8)$. Over the range of H that is explored, we find that the agreement between the experimental data and the analytical model is excellent without any adjustable parameter. Note that we observe a slight discrepancy between the value of B provided by the model and the experimental data for small diameter values $d = 5$ mm (Fig. 4b). This slight discrepancy is also observed in the infinite case (Fig. 2). We believe that this deviation is linked to the fact that the granular medium can no longer be considered as a continuous medium, as the aspect ratio between sphere diameter and grain diameter begins to approach 1.

Agreement between the model and the experimental allows us to specify the influence of K_z and K_v in the model. Indeed, it can be seen that the K_v term has not been modified from the infinite case to obtain this agreement. This is consistent with the modeling of a collisional drag force term [18, 24, 25]. This term has no connection with friction at a wall. The most striking feature is that K_z can be kept constant when using lateral confinement. The value of K_z is closely linked to the macroscopic coefficient of friction between the grains. The presence of lateral walls can certainly generate a different coefficient of friction between the grains and the walls, but this difference will often be of the same order of magnitude, as is the case in the experimental measurements. It is not reasonable to expect an exponential variation in the coefficient of friction in the experimental data. Thus, the presence of a wall modifies the pressure prevailing within the granular medium through a geometric effect due to grain chaines forces clinging to the lateral walls.

The model allows also to describes the data in a refined way as already specified in expererimental study [8]. In this study, the fits were established without a model equation, with the goal of describing the data as well as possible. The fits were chosen in exponential form to account for the growth of α and B at low values of Λ and the saturation of α and B at high values of Λ. We find that the fit of $\alpha(\Lambda)$ proposed by [8] has a rather acceptable form (Fig. 4a). However, the fit of $B(\Lambda)$ deviates significantly from the model for low values of Λ (Fig. 4b). In particular, the fit proposes a non-zero value of B when $\Lambda = 0$, whereas the model specifies that $B(\Lambda = 0) = 0$. The model derived from equation 4 provides an improvement on what was identified in the experimental data.

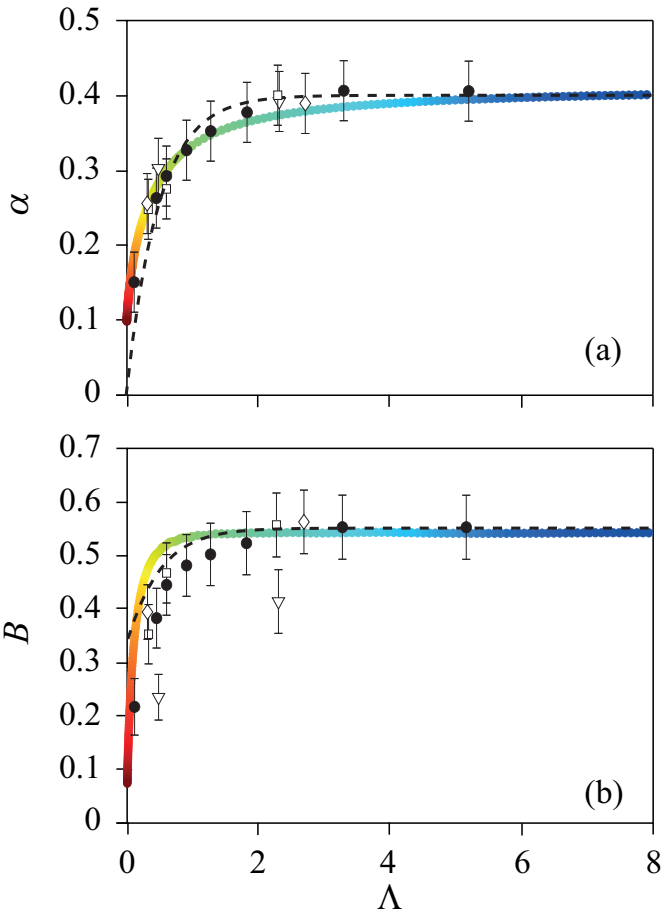

Fig. 4: Power exponent α (a) and Prefactor B (b) of Eq. 6 as a function of Λ obtained by solution of Eq. 4. The color code corrreponds to increasing values of Λ and is the same as in figure 2. The symbols corresponds to experimental data in the same configuration, extracted from [8]. For varying D and $\rho = 7800$ kg.m^{-3}, ($\triangledown$) $d = 5$ mm, ($\bullet$) $d = 19$ mm and ($\square$) $d = 40$ mm. For $\rho = 14970$ kg.m^{-3}, ($\diamond$) $d = 20$ mm. The dashed lines correspond to the best fit of the experimental data described by [8].

Conclusion. – In this study, we investigated analytically the penetration depth of spheres by impact in a confined granular medium. Experimental scaling laws in the form of power laws are useful to foresee penetration depth [8, 15, 16]. They are self-explanatory and do not require equation solving. However, they are only valid for a certain range of impact velocities and geometric dimensions. Complete equation-based modeling of the problem enriches experimental results by allowing them to be supplemented. For example, it is possible to take into account the effects of lateral confinement by correcting the hydrostatic pressure-type term in granular materials. This correction involves an exponential expression [26]. The incorporation of this term in the penetration dynamics equations makes it possible to account for the effect of confinement on penetration depth. The results obtained analytically are in excellent agreement with the experimental results. The inclusion of confinement effects enriches dynamic models of object penetration and gives new insights on the physics of geotechnical situation, industrial prob-

lems and locomotion in granular materials.

Acknowledgement. – We thank P. Gondret and J. Vatteville for fruitful discussions and for their reading of the manuscript.

***.** – REFERENCES

[1] MJ Forrestal and VK Luk. Penetration into soil targets. *International Journal of Impact Engineering*, 12(3):427–444, 1992.

[2] C Glößner, S Moser, R Külls, S Heß, S Nau, M Salk, D Penumadu, and N Petrinic. Instrumented projectile penetration testing of granular materials. *Experimental Mechanics*, 57:261–272, 2017.

[3] H Jay Melosh. Impact cratering: A geologic process. *New York: Oxford University Press; Oxford: Clarendon Press*, 1989.

[4] Stuart J Robbins and Brian M Hynek. A new global database of mars impact craters 1 km: Database creation, properties, and parameters. *Journal of Geophysical Research: Planets*, 117(E5), 2012.

[5] Sandesh Kamath, Yaping Shao, and Eric JR Parteli. Scaling laws in aeolian sand transport under low sand availability. *Geophysical Research Letters*, 49(11):e2022GL097767, 2022.

[6] Amanda M Walsh, Kristi E Holloway, Piotr Habdas, and John R de Bruyn. Morphology and scaling of impact craters in granular media. *Physical review letters*, 91(10):104301, 2003.

[7] J R de Bruyn and A M Walsh. Penetration of spheres into loose granular media. *Canadian Journal of Physics*, 82(6):439–446, 2004.

[8] Antoine Seguin, Yann Bertho, and Philippe Gondret. Influence of confinement on granular penetration by impact. *Physical Review E*, 78(1):010301, 2008.

[9] Stéphanie Deboeuf, Philippe Gondret, and Marc Rabaud. Dynamics of grain ejection by sphere impact on a granular bed. *Physical Review E*, 79(4):041306, 2009.

[10] Paul Umbanhowar and Daniel I Goldman. Granular impact and the critical packing state. *Physical Review E*, 82(1):010301, 2010.

[11] JO Marston, EQ Li, and Sigurdur T Thoroddsen. Evolution of fluid-like granular ejecta generated by sphere impact. *Journal of fluid mechanics*, 704:5–36, 2012.

[12] Hiroaki Katsuragi. *Physics of soft impact and cratering*. Springer, 2016.

[13] Devaraj Van Der Meer. Impact on granular beds. *Annual Review of Fluid Mechanics*, 49:463–484, 2017.

[14] F Pacheco-Vázquez. Ray systems and craters generated by the impact of nonspherical projectiles. *Physical review letters*, 122(16):164501, 2019.

[15] JS Uehara, MA Ambroso, RP Ojha, and Douglas J Durian. Low-speed impact craters in loose granular media. *Physical Review Letters*, 90(19):194301, 2003.

[16] MA Ambroso, Randall D Kamien, and Douglas J Durian. Dynamics of shallow impact cratering. *Physical Review E*, 72(4):041305, 2005.

[17] Douglas D Carvalho, Nicolao C Lima, and Erick M Franklin. Roles of packing fraction, microscopic friction, and projectile spin in cratering by impact. *Physical Review E*, 107(4):044901, 2023.

[18] Hiroaki Katsuragi and Douglas J Durian. Unified force law for granular impact cratering. *Nature physics*, 3(6):420–423, 2007.

[19] Antoine Seguin, Yann Bertho, Philippe Gondret, and Jérôme Crassous. Sphere penetration by impact in a granular medium: A collisional process. *EPL (Europhysics Letters)*, 88(4):44002, 2009.

[20] John Hinch. Particles impacting on a granular bed. *Journal of Engineering Mathematics*, 84(1):41–48, 2014.

[21] Junke Guo. Exact solution for depth of impact crater into granular bed. *Journal of Engineering Mechanics*, 144(1):06017018, 2018.

[22] R. Albert, M. A. Pfeifer, A.-L. Barabási, and P. Schiffer. Slow drag in a granular medium. *Phys. Rev. Lett.*, 82:205–208, Jan 1999.

[23] Istvan Albert, JG Sample, AJ Morss, S Rajagopalan, A-L Barabási, and P Schiffer. Granular drag on a discrete object: Shape effects on jamming. *Physical Review E*, 64(6):061303, 2001.

[24] Yuka Takehara, Sachika Fujimoto, and Ko Okumura. High-velocity drag friction in dense granular media. *EPL (Europhysics Letters)*, 92(4):44003, 2010.

[25] Yuka Takehara and Ko Okumura. High-velocity drag friction in granular media near the jamming point. *Physical Review Letters*, 112(14):148001, 2014.

[26] Guillaume Ovarlez, Evelyne Kolb, and Eric Clément. Rheology of a confined granular material. *Physical Review E*, 64(6):060302, 2001.

[27] Yann Bertho, Frédérique Giorgiutti-Dauphiné, and Jean-Pierre Hulin. Dynamical janssen effect on granular packing with moving walls. *Physical Review Letters*, 90(14):144301, 2003.

[28] LA Lopez-Rodriguez and F Pacheco-Vazquez. Friction force regimes and the conditions for endless penetration of an intruder into a granular medium. *Physical Review E*, 96(3):030901, 2017.

[29] Shivam Mahajan, Michael Tennenbaum, Sudhir N Pathak, Devontae Baxter, Xiaochen Fan, Pablo Padilla, Caleb Anderson, Alberto Fernandez-Nieves, and Massimo Pica Ciamarra. Reverse janssen effect in narrow granular columns. *Physical Review Letters*, 124(12):128002, 2020.

[30] Antoine Seguin, Yann Bertho, and Baptiste Darbois Texier. Penetrating a granular medium by successive impacts. *Physical Review E*, 106(5):054904, 2022.

[31] H.A. Janssen. *Z. Ver. Dtsch. Ing.*, 39:1045, 1895.

[32] Farhang Radjai, Michel Jean, Jean-Jacques Moreau, and Stéphane Roux. Force distributions in dense two-dimensional granular systems. *Physical review letters*, 77(2):274, 1996.

[33] MB Stone, R Barry, DP Bernstein, MD Pelc, YK Tsui, and P Schiffer. Local jamming via penetration of a granular medium. *Physical Review E*, 70(4):041301, 2004.

[34] A Seguin and P Gondret. Buckling of a rod penetrating into granular media. *Physical Review E*, 98(1):012906, 2018.

[35] Wenting Kang, Yajie Feng, Caishan Liu, and Raphael Blumenfeld. Archimedes' law explains penetration of solids into granular media. *Nature communications*, 9(1):1–9, 2018.

[36] B Darbois Texier and A Seguin. Successive reintrusions in a granular medium. *Physical Review E*, 106(1):014906, 2022.